Colloids and Surfaces B: Biointerfaces 260 (2026) 115398

Contents lists available at ScienceDirect

Colloids and Surfaces B: Biointerfaces

journal homepage: www.elsevier.com/locate/colsurfb

A fluorescein-tagged pH-low insertion peptide (pHLIP) for glioblastoma imaging: Lipid membrane interaction and cancer cell targeting

Cristina Chirizzi [a,b,*], Martina Maffezzini [c,d], Nadia Mosca [a], Arianna Balestri [e], Costanza Montis [e], Francesco Acerbi [f,g,h,i], Martina Beccalli [a], Alessandro Gori [j], Marina Grisoli [b], Serena Pellegatta [c,d,**], Francesca Baldelli Bombelli [a,***]

[a] SupraBioNanoLab, Department of Chemistry, Materials, and Chemical Engineering "Giulio Natta", Politecnico di Milano, Milano 20131, Italy
[b] Neuroradiology Unit, Fondazione IRCCS Istituto Neurologico Carlo Besta, Via Celoria 11, 20133 Milan, Italy
[c] Unit of Immunotherapy of Brain Tumors, Fondazione IRCCS Istituto Neurologico Carlo Besta, Via Celoria, 11, Milan 20133, Italy
[d] Unit of Neuro-Oncology, Fondazione IRCCS Istituto Neurologico Carlo Besta, Milan 20133, Italy
[e] Department of Chemistry "Ugo Schiff" and CSGI, University of Florence, Florence, Italy
[f] Neurosurgical Unit 2, Department of Neurosurgery, Fondazione IRCCS Istituto Neurologico Carlo Besta, Milan, Italy
[g] Experimental Microsurgical Laboratory, Department of Neurosurgery, Fondazione IRCCS Istituto Neurologico Carlo Besta, Milano, Italy
[h] Neurosurgery Unit, Pisa University Hospital, Italy
[i] Department of Translational Medicine and New Technologies in Medicine and Surgery, University of Pisa, Pisa University Hospital, Italy
[j] National Research Council of Italy, Istituto di Scienze e Tecnologie Chimiche (SCITEC-CNR), Milan, Italy

ARTICLE INFO

Keywords:
Glioblastoma
PH-responsive peptides
Lipid membranes
Biointerfaces
Fluorescein
Tumor microenvironment (TME)

ABSTRACT

Glioblastoma (GB) is the most aggressive and common malignant brain tumor, and despite current therapeutic approaches, prognosis remains poor. Given that surgical resection is frequently the sole potentially curative option, precise intraoperative tumor delineation is crucial for reducing recurrence rates and enhancing patient outcomes. In this study, we developed a novel pH-responsive imaging tool by coupling the pH-low insertion peptide (pHLIP) with fluorescein (FL) to enable targeted fluorescence-guided visualization of tumor margins. We investigated pHLIP–lipid membrane interactions using model systems, including liposomes and supported lipid bilayers (SLB), assessing peptide's pH-dependent insertion mechanism. Complementary *in vitro* experiments on patient-derived GB cell lines were performed to show the tracer's pH sensitivity, selective membrane targeting, and potential off-target effects. The FL-pHLIP construct showed robust, pH-dependent membrane insertion and selectivity in GB cellular models with minimal interaction under physiological conditions. These findings support FL-pHLIP as a promising candidate for fluorescence-guided surgery in GB and highlight its potential for clinical translation and for the broader development of pH-responsive diagnostic tools.

1. Introduction

Glioblastoma (GB) is the most common and deadliest primary malignant brain cancer, accounting for approximately 17 % of all diagnosed tumors [1]. Despite optimal treatment, outcomes remain poor, with recurrence rates reaching 88.8 % within two years and a median survival of just 18.8 months [2]. Moreover, the intrinsic aggressiveness of GB, combined with therapeutic resistance and marked intratumoral heterogeneity, enhanced by invasive behavior and an immunologically "cold" tumor microenvironment (TME) [3], presents major challenges for both effective treatment and accurate surgical delineation. Consequently, identifying a universal TME-associated biomarker resilient to GB heterogeneity and invasiveness is essential for developing improved therapeutic strategies. Among the available candidates, acidic pH has gained increasing attention. Cancer cells maintain intracellular pH homeostasis, which creates a persistently acidic extracellular environment at the cell surface. This acidity is markedly lower than physiological pH and remains evident even in well-perfused tumor regions [4,5]. As a

* Corresponding author at: Neuroradiology Unit, Fondazione IRCCS Neurologico Carlo Besta, Via Celoria, 11, Milan 20133, Italy.
** Corresponding author at: Unit of Immunotherapy of Brain Tumors, Fondazione IRCCS Istituto Neurologico Carlo Besta, Via Celoria, 11, Milan 20133, Italy.
*** Correspondence to: Department of Chemistry, Materials, and Chemical Engineering "Giulio Natta", Politecnico di Milano, via Bassini 7, Milano 20133, Italy.
E-mail addresses: cristina.chirizzi@istituto-besta.it (C. Chirizzi), serena.pellegatta@istituto-besta.it (S. Pellegatta), francesca.baldelli@polimi.it (F. Baldelli Bombelli).

https://doi.org/10.1016/j.colsurfb.2025.115398
Received 11 November 2025; Received in revised form 16 December 2025; Accepted 23 December 2025
Available online 24 December 2025

result, surface acidity represents a distinctive and targetable feature of cancer, with significant potential for improving preoperative tumor mapping. Although recent progress in biodegradable biopolymers and nanoparticle-based delivery systems has expanded the range of tools available for cancer targeting and imaging [6–9], their clinical translation is often limited by concerns related to long-term biodistribution, degradation products, and off-target accumulation [10]. These considerations highlight the need for simpler, well-defined, and biologically compatible targeting systems, such as peptide-based probes, which offer improved predictability and safety profiles. Accordingly, we employed well-established molecules, such as pH-low insertion peptides (pHLIPs), to target acidic tumors and deliver imaging agents to cancer cells. Due to their moderate hydrophobicity, pHLIPs exhibit a modest affinity for cellular membranes at physiological pH, while at lower pHs (< 7) they undergo a specific folding promoting their insertion in phospholipid bilayers. This enables them to detect pH changes on the surface of diseased tissues, where acidity is highest, and preferentially embed into the cellular membrane [11–13]. These peptides can be employed in a broad range of applications, including therapeutic needs [14–16], enhancement of nanoparticle delivery to cancer cells and imaging purposes [17,18], such as labelling primary tumors and submillimeter-sized metastatic lesions in contexts other than GB [19–22], with ongoing translation into clinical practice (ClinicalTrials.gov identifier: NCT05130801).

Considering that optical fluorescence imaging has emerged as a cost- and time-efficient technique for accurately guiding brain surgery and maximizing tumor resection [23,24], we propose a novel selective fluorescent tracer based on the combination of a pHLIP with fluorescein (FL). Despite being a pH-sensitive dye with reduced sensitivity in acidic conditions [25], the choice of FL has been driven by its use in clinical practice. In fact, the integration of FL-specific filters (surgical microscope filter YELLOW 560 nm) has improved FL-guided microsurgery by providing enhanced visualization and differentiation of tumor tissues. In addition, unlike other dyes such as 5-aminolevulinic acid (5-ALA) [26] and indocyanine green (ICG) [27], which are administered well in advance of the procedure, FL is administered during anesthesia, making it a particularly safe and effective option, especially for challenging, deep-seated surgical fields. However, the effectiveness of FL tissue staining is contingent upon extracellular accumulation resulting from the disruption of the blood-brain barrier (BBB). This could reduce its accuracy in tumoral tissue identification, with a potential impact on intra-operative discrimination between cancer border and peritumoral area during resection. By conjugating FL to pHLIP, for the first time, we aim to enhance its selective uptake in tumor tissues, thereby improving the accuracy of intra-operative tumor identification [28,29]. The primary goal of this study is to utilize a well-established pHLIP strategy for the targeted delivery of fluorescein into tumor tissues, aiming to enhance the accuracy of intraoperative delineation of GB margins. To evaluate the efficiency of this approach, we examined the capability of FL-pHLIP to insert into lipid membrane model systems and cell membranes as a function of pH. We first used a simplified membrane model system, such as supported lipid bilayers (SLB), to study the pH-sensitive insertion mechanism as a function of time and pH by quartz crystal microbalance with dissipation (QCM-D) technology and fluorescence confocal microscopy. We then validated these results by *in vitro* experiments performed on primary cell lines derived from newly diagnosed GB patients.

Our study introduces the first FL-pHLIP derivative and reports a very comprehensive physicochemical investigation of its interaction with lipid membranes and primary GB cells. The obtained results show that FL functionalization does not affect pHLIP folding, binding kinetics, and stability across relevant pH conditions. Notably, our findings also demonstrate that the excellent insertion selectivity of this derivative at pH < 7 in the relevant biological environment effectively compensates for the observed significant decrease in fluorescence intensity supporting its translational potential. Considering the highly promising obtained outcomes, *in vivo* validation is currently underway to further explore FL-pHLIP clinical potential. Success in this direction could significantly enhance intraoperative tumor visualization, with a subsequent impact on both extent of resection and patient survival. Moreover, our findings provide a valuable proof of concept for extending this peptide-based approach to other aggressive tumors characterized by an acidic pH of the TME, similar to that observed in GB.

2. Experimental section

2.1. Materials

Dulbecco's Phosphate - Buffered Saline 0.01 M pH 7.4 (DPBS, Corning, NY, USA); Acetate buffer 0.1 M pH 5.2 (prepared with $C_2H_3NaO_2$ and $C_2H_4O_2$ in deionized water according to Henderson–Hasselbalch equation); TRIS buffer 0,1 M pH 6.5 (prepared from TRIS powder, ≥99.8 %, Bio Rad, in deionized water); Acetic acid ($C_2H_4O_2$, ≥99.7 %, ACS reagent, Sigma Aldrich, Germany); Chloroform ($CHCl_3$, ≥99.5 %, Sigma Aldrich, Germany); Water ultrapure Type-I Milli-Q Water provided by a Simplicity® water purification system.

All pHLIP peptides (WT: AEQNPIYWARYADWLFTTPLLLLD LALLVDADEGT; FL-derivative: *ACEQNPIY WARYADWLFTTPLLLLDLA LLVDADEGT*, and SC-FL construct (scrambled-fluorescein construct): *ACEQNPIY WARYAKWLFTTPLLLLKLALLVDAKEGT* were kindly synthesized by Dr. Alessandro Gori from "Istituto di Scienze e Tecnologie Chimiche "Giulio Natta" (SCITEC) of National Research Council (CNR, Milan, Italy); Sodium phosphate monobasic (H_2NaO_4P, ≥98 %, Bio-Reagent, Sigma Aldrich, Germany); Sodium phosphate dibasic (HNa_2O_4P, ≥99 %, ACS reagent, Sigma Aldrich, Germany); Sodium acetate ($C_2H_3NaO_2$, ≥99 %, analytical reagent, Prolabo); Calcium chloride ($CaCl_2$, ≥97 %, Sigma Aldrich); 1,2-dioleoyl-sn-glycero-3-phosphocholine (18:1 (Δ9-Cis) PC (DOPC), MW 786.113 g/mol, Avanti Polar Lipids, USA).

2.2. Synthesis of pHLIPs

Peptides were assembled by stepwise microwave-assisted Fmoc-SPPS on a Biotage ALSTRA Initiator+ peptide synthesizer, operating in a 0.12 mmol scale on a pre-loaded 2-CTC resin (0,6 mmol/g). Resin was swelled prior to use with an NMP/DCM mixture. Activation and coupling of Fmoc-protected amino acids were performed using Oxyma 0.5 M / DIC 0.5 M (1:1:1), with 5 equivalents in excess over the initial resin loading. Coupling steps were performed for 10 min at 50 °C. Deprotection steps were performed by treatment with a 20 % piperidine solution in DMF at room temperature (1 × 3 min + 1 × 5 min). Following each coupling or deprotection step, peptidyl-resin was washed with DMF (4×5 mL). The final peptide chain was cleaved from the resin using a TFA 90 %, water 5 %, thioanisole 2.5 %, TIS 2.5 % mixture (3 h, RT). Following precipitation in cold diethyl ether, the crude peptide was collected by centrifugation and washed with further cold diethyl ether to remove scavengers. Peptides were then dissolved in a 50 % aqueous acetonitrile 0.07 % TFA buffer and purified by preparative RP-HPLC. Pure RP-HPLC fractions (>95 %) were combined and lyophilized. Mass spectra were collected separately.

2.3. pHLIP solubilization and UV-visible analysis

pHLIP WT/FL-pHLIP stock solutions were prepared by dissolving the peptide at physiological pH in 0.01 M Phosphate-Buffered Saline (PBS). The optimized procedure was effective for both systems and involved the following experimental steps:

1) Dissolution of the peptides in PBS by vortexing to prepare a 100 μM stock solution.
2) The resulting solution was heated to 35 °C for 30 min and fully dissolved using an ultrasonic bath (5 min at 59 kHz).

The same procedure was then used for preparing pHLIP WT/FL-pHLIP stock solutions in 0.1 M acetate buffer and 0.1 M Tris buffer to achieve pH values of 5.2 and 6.5, respectively.

The correct solubilization of pHLIP was checked for each newly prepared pHLIP stock solution by UV-Vis spectroscopy by comparison to a calibration curve. The UV-Vis profile of pHLIPs was characterized in detail as follows. The absorbance (Abs) of the WT peptide was analyzed over the range of 200–500 nm, with the maximum signal observed at 280 nm. Similarly, the absorbance of FL-pHLIP was recorded over the same range, also showing a maximum at 280 nm. Each measurement was performed in triplicate to ensure proper statistical significance.

2.4. Liposomes preparation

DOPC unilamellar vesicles used as model membranes to study peptide-lipid interaction were prepared through the film rehydration method. DOPC was dissolved in chloroform at a concentration of 20 $mg{\cdot}mL^{-1}$ and dried by rotary evaporation at 30 °C to produce a thin film. The resulting DOPC film was rehydrated in 0.01 M PBS, 0.1 M Tris, or 0.1 M Acetate buffer at pH 7.4, 6.5, and 5.2, respectively, depending on the application. Freeze-thaw cycles were repeated 5 times by dipping the hydrated film in liquid nitrogen and then heating the solution at 50 °C to break the multilayer structures and only form unilamellar vesicles. The resulting liposome dispersion was sequentially extruded through 200 nm and 100 nm polycarbonate filters (11 times/each filter). To verify proper liposome formation, dynamic light scattering (DLS) analysis was performed on samples diluted 1:50 (v/v) in the corresponding hydration buffer, as described below.

2.5. Dynamic light scattering (DLS)

DLS measurements were performed using an ALV apparatus equipped with an ALV-5000/EPP correlator, a special optical fiber detector, and an ALV/CGS-3 compact goniometer. The light source was a He-Ne laser ($\lambda = 633$ nm) with an output power of 22 mW. In this study, DLS was utilized to characterize peptide self-assembly and exclude possible aggregation. Single-angle DLS measurements at 90 ° were conducted at a controlled temperature of 25 °C. For the stability assays of both WT and FL-pHLIPs, 90 ° DLS measurements were carried out on 0.8 mL of 5 μM peptide solutions at different pH values (7.4, 6.5, and 5.2) and at distinct time points (fresh (T_0, 30 min, 1 h, 2 h, and 24 h). Specifically, a 100 μM peptide stock solution was diluted 1:20 v/v in 0.1 M acetate buffer, 0.1 M Tris, or 0.01 M PBS to achieve pH values of 5.2, 6.5, and 7.4, respectively. Each measurement was recorded for 5–10 s with a sensitivity threshold of 10 %, and the apparent hydrodynamic radius was estimated via intensity-unweighted fitting of the autocorrelation function.

For liposome characterization, the z-averaged hydrodynamic diameter (D_H) was extrapolated from values obtained by cumulant fitting of the autocorrelation functions measured at scattering angles (θ) of 70 °, 90 °, 110 °, and 130 °. The intensity-weighted size distribution at $\theta = 90$ ° was obtained through CONTIN analysis of the corresponding autocorrelation function. For these measurements, the stock solution was diluted 1:50 v/v in water and analyzed at 25 °C.

2.6. Circular Dichroism spectroscopy

The interaction of WT and FL-pHLIPs with DOPC liposomes was first analyzed by Circular Dichroism (CD), which made it possible to estimate peptide folding and, therefore, to verify their pH-dependent penetration into the lipid bilayer. CD measurements were performed by a Jasco® J-815 CD spectrometer. Spectra were recorded in a wavelength range between 200 and 260 nm, with steps of 1 nm and a scanning speed of 100 nm/min. Solutions containing 5 μM pHLIP (for both WT- and FL-derivatives) and 750 μM DOPC liposomes were measured at different pH values (7.4, 6.5, and 5.2) after a 15-minute incubation period against a buffer baseline. Specifically, peptide stock solutions (100 μM) were diluted 1:20 v/v in 0.1 M acetate buffer for pH 5.2, and in 0.1 M Tris or 0.01 M PBS for pH 6.5 and 7.4, respectively. Similarly, solutions containing 5 μM FL-pHLIP and 750 μM DOPC liposomes were measured at different pH values (7.4, 6.5, and 5.2) and time points (30 min, 2 h, and 4 h) against a buffer baseline. All measurements were averaged over 10 acquisition runs.

2.7. Fluorescein quantum yield (Φ) determination

To determine the quantum yield of fluorescein at different pH values (7.4 and 6.7, representative of the tumor microenvironment in glioblastoma), solutions of fluorescein salt (Sigma Aldrich, Germany) were prepared in phosphate-buffered saline (PBS) at four concentrations: 1.5, 2.5, 5, and 10 mM, with the pH adjusted according to the target value. A fluorescein salt solution in HEPES buffer (10 mM, pH 7.4), with a known quantum yield of 0.89, was used as a reference.

For fluorescence measurements, samples were excited at the peak absorbance wavelength of 490 nm, and emission spectra were collected using a Jasco® FP-8500 Spectrofluorometer. The integrated fluorescence intensities for each sample were compared to the standard solution. To ensure accurate quantum yield calculations, the absorbance (A) of the same samples was measured at the FL excitation wavelength (490 nm). A values were maintained below 0.1 for each sample to avoid inner filter effects and to ensure a linear relationship between absorbance and concentration. The quantum yield (Φ) was calculated using the following formula:

$$\Phi\text{sample} = \Phi\text{standard}.\left(\frac{I_{sample}}{I_{standard}}\right).\quad\left(\frac{A_{\ sample}}{A_{sample}}\right).\left(\frac{n^2_{sample}}{n^2_{standard}}\right)$$

Where:

I_{sample} and $I_{standard}$ represent the integrated fluorescence intensities of the sample and the standard, respectively, while A_{sample} and $A_{standard}$ are the absorbance values at the excitation wavelength (490 nm). Finally, n indicates the refractive index of the solvent for the reference (standard) and the sample, respectively. Absorbance measurements for each sample were performed in a 1 cm path-length cuvette.

2.8. QCM-D surface preparation

Before each use, SiO_2-coated chips (QSX 303 by Biolin) were cleaned and prepared for QCM-D analysis following a specific protocol. First, the chips were immersed in a 2 % w/v aqueous solution of Sodium Dodecyl Sulphate (SDS) for 15 min, then rinsed with ultra-purified water (MilliQ) and 70 % ethanol. They were subsequently dried under a stream of nitrogen gas and treated in a UV-Ozone chamber for 15 min. Immediately after each measurement, the crystals were cleaned with SDS solution for 15 min, rinsed with MilliQ water and 70 % ethanol, dried under nitrogen, and stored until reuse.

2.9. Quartz crystal microbalance analysis

QCM-D experiments were performed using a dissipative QCM instrument (Q-Sense E4, Biolin Scientific AB, Sweden) equipped with a flow-through system and a peristaltic pump. After the sensor cleaning procedure, the QCM system was tared through a two-step calibration process. First, air calibration was performed automatically by the software, followed by solvent calibration using MilliQ water to fully fill the chamber and cover the sensors. Once both calibrations were completed, the QCM-D system was ready for measurement.

During the first 5 min of the measurement, a baseline was acquired using 0.01 M PBS as solvent. Supported lipid bilayers (SLBs) were then formed through the adsorption and rupture of lipid vesicles (DOPC solution at a concentration of 0.25 mg mL^{-1} in $CaCl_2$ buffer) on the cleaned SiO_2 surfaces. The solution was flowed through each QCM

chamber for 8 min at a rate of 0.1 mL min^{-1}. The same flow rate was maintained throughout the entire duration of the experiment. PBS 0.01 M was introduced again for 5 min, followed by a 5-minute flow of MilliQ water to remove excess lipids and stabilize the bilayer. A unilamellar SLB is properly formed if the frequency reaches a value of around −25 Hz with an associated dissipation below 1 and tending to 0 for a more rigid system [30]. The superimposition of the different harmonics also confirms the rigidity of the system. After proper SLB formation, to optimize the environment for studying pHLIP-membrane interactions, the final 5-minute flow of MilliQ water was followed by 15 min of the buffer used for the QCM-D experiment. Specifically, 0.1 M Acetate, 0.1 M TRIS buffer, or 0.01 M PBS were used for analyses at pH 5.2, 6.5, and 7.4, respectively. Lastly, the peptide solution, previously diluted in the appropriate buffer according to the studied pH, was introduced into the system for a specified timing. Following this, the pump was turned off to allow for static incubation. Finally, the system was washed with the same buffer used to dissolve pHLIP. Detailed procedural steps are provided below. Each experiment was repeated at least three times.

Experimental conditions

[pHLIP] (μM)	*FL-pHLIP flow time (min)*	*Static incubation (min)*	*Washing time (min)*
0.5	15	15	15

2.10. In vitro cellular experiments

FL-pHLIP tolerance and its binding efficacy were finally evaluated on primary cell lines from newly diagnosed GB, growing *in vitro* as neurospheres [31] at different pHs (7.4 and 6.5). These cells were derived from fresh tumor tissues provided from cases operated in the Department of Neurosurgery of Fondazione IRCCS Istituto Neurologico "Carlo Besta" (FINCB). Written informed consent was obtained from all patients. Tumor samples were processed to derive primary GB cell lines as previously described [31,32], using a combination of mechanical dissociation and enzymatic disaggregation. Primary cell lines were successfully established in 65–70 % of cases, particularly from CUSA surgical materials. Debris might still be present in the culture until passage 4–6 (p4–6). Even if debris does not disturb the growth of cells, it could affect the peptide performance. Considering that, GB primary cell lines were used within passages p6-p10.

For cell culture maintenance, a DMEM/F-12, GlutaMAX (Dulbecco's Modified Eagle Medium/Nutrient Mixture F-12; Gibco, Thermo Fisher, MA, USA) medium containing a B27 supplement (1X, Thermo Fisher Scientific) was used, along with 100 mg/mL streptomycin, 100 U/mL penicillin, 0.25 μg/mL Fungizone (Gibco, Thermo Fisher Scientific, MA, USA), and 20 ng/mL of mitogenic factors EGF and bFGF (basic fibroblast growth factor, PeproTech). To prepare the acidic environment, the selected cells were grown for several days. Thus, their metabolic activity was enhanced, and it caused a reduction in the extracellular pH. The acid culture medium, thus obtained, was then collected, stored at −20 °C, and used at the time of the cellular experiment for the duration of peptide incubation.

Specifically, for FL-pHLIP cellular staining, cells were cultured at a density of 200k cells/well in a 48-well plate and with the peptide for 2 h at different concentrations (0.5 μM, 5 μM, and 10 μM) after mechanical dissociation into single cells. Both acid (pH 6.4 – 6.7) and physiological conditions (pH 7.2 – 7.4) were investigated. After incubation, the cells were washed in their respective culture media (acidic or physiological pH) to remove unbound peptide (3 × 1000 rpm for 5 min). Cell viability and pHLIP tolerance were assessed using 7-Aminoactinomycin D (7-AAD) staining and analyzed via flow cytometry (FACS). A scrambled peptide (SC-FL pHLIP; ACEQNPIYWARYAKWLFTTPLLLLKLALL VDAKEGT), which is not pH-sensitive, was used as a control and subjected to the same procedures.

The amount of inserted fluorescent peptide was quantified by measuring the mean fluorescence intensity of cells positive for pHLIP through FACS analysis. Acquisitions were performed using a MACSQuant (Miltenyi Biotec) flow cytometer, and data were analyzed using the FlowLogic software (version 7.2, Miltenyi Biotec).

2.11. Confocal analyses on SLB surfaces and primary glioblastoma cells

For experiments on FL-pHLIP interaction with SLBs, the SLBs were prepared directly on an 8-well chamber slide (Nunc™ Lab-Tek™ Chambered Coverglass, Thermofisher Scientific) and analyzed. Small Unilamellar Vesicles were prepared as described in section 2.4. A solution of 10 mM $CaCl_2$ was first applied to the surface of the chamber slide, followed by the addition of a 10 mM vesicle dispersion. A stable SLB layer on the chamber slide was achieved by rinsing the vesicle dispersion with pure Milli-Q water after 30 min of incubation at room temperature. To fluorescently label the SLB, a small amount of fluorescent probes (Cy5, Sulfo-Cyanine5), *i.e.*, 0.1 % mol: mol with respect to total lipid amount, was added. After SLB formation, it was stabilized in the buffer under study for several minutes, then replaced with a 0.5 μM solution of FL-pHLIP at specific pH values (7.4, 6.5, and 5.2) and incubated for 30 min. Following incubation, the SLB was washed three times with the corresponding buffer and left in the same solution. These experiments were carried out with a laser scanning confocal microscope, Leica TCS SP8 (Leica Microsystems GmbH, Wetzlar, Germany) equipped with a 63 × water immersion objective.

For experiments on primary GB cell lines, the efficacy of FL-pHLIP variants was first quantified by flow cytometry and subsequently confirmed via confocal microscopy. Cells were cultured at a density of 50000 cells per well on 15 mm round cover glasses placed in 24-well plates. Before incubation, the cover glasses were coated with laminin (10 μg/mL, Sigma Aldrich, Germany) to promote cell adhesion. Cells were then incubated with 5 μM FL-pHLIP for 2 h at either physiological or acidic pH (pH 6.5). Following incubation, the cells were washed three times with their respective culture media (acidic or physiological) to remove any unbound peptide and then fixed with 4 % w/v paraformaldehyde (PFA, Sigma Aldrich, Germany). For confocal microscopy, cells were treated with 1 % BSA (Santa Cruz Biotechnology) and incubated in a humidified chamber with the anti-B7H3 goat antibody (1:100 dilution, R&D Systems) for 1 h at room temperature. Detection of B7H3 was achieved using Alexa Fluor 594-conjugated goat anti-rabbit antibody (1:50 dilution, Thermo Fisher Scientific). Cell nuclei were counterstained with DAPI (Sigma Aldrich, Germany), and the cover glasses were mounted with FluorSave mounting medium (Sigma Aldrich, Germany). Confocal imaging was performed using a Leica TCS SP8 laser scanning confocal microscope (Leica Microsystems GmbH, Wetzlar, Germany).

2.12. Statistical analysis

All measurements presented in this work are reported as the mean ± standard deviation, based on a minimum of $n = 3$ replicates for each condition. Cellular experiments were performed at least twice, with each assay containing three technical replicates. Data were analyzed using Prism Software (GraphPad Software version 9), and statistical significance was assessed using the Student's *t*-test. Specifically, this method was used to determine whether there was a significant difference between the mean of two groups (physiological and acidic pH). Statistical significance was defined as $p < 0.05$.

3. Results and discussion

3.1. Peptide solubility and chemical-physical properties

In this study, we examined two variants of the pHLIP peptide: 1) The wild type (WT), which is defined by the well-characterized sequence

AEQNPIYWARYADWLFTTPLLLLDLALLVDADEGT and 2) a fluorescently labeled derivative, obtained by chemically attaching fluorescein (FL) to a cysteine residue at the peptide's N-terminal via a short disulfide linker, designated as FL-pHLIP. WT-pHLIP was our control for evaluating the desired pH-responsive properties of the newly developed FL-pHLIP from the perspective of using it as a tracer in the TME during surgical interventions.

We first assessed the solubility/dispersibility of WT-pHLIP in physiological conditions (*i.e.,* saline phosphate buffer at pH=7,4 - PBS) by incrementally adding small volumes of PBS to a fixed amount of peptide. Experimental results indicated that homogeneous dissolution/dispersibility was achieved only by heating the sample, combined with vortex mixing and bath sonication, as detailed in Table 1. The maximum concentration of WT-pHLIP that could be effectively dissolved/dispersed in the physiological medium was 0.6 mM, equivalent to 2.5 mg mL^{-1}.

Building on these observations, we optimized a solubilization protocol outlined in 6 of the Methods. This approach was designed to ensure high reproducibility by utilizing concentrations significantly lower than the previously established solubility/dispersibility limits. The same study was extended to the FL-pHLIP variant. The dispersions appeared clear and without visible agglomerates and/or precipitates. The dissolution/dispersibility efficiency of both pHLIPs was assessed by UV-Vis analysis (Figure S1A-B). This procedure ensured that the solubilized/dispersed peptide was accurately quantified in all freshly prepared stocks.

.

Subsequent studies were performed to evaluate pHLIP self-assembly upon dissolution at different pH levels. Self-assembling behavior of both derivatives was studied through DLS measurements, dissolving both peptides in 0.1 M acetate buffer, 0.1 M Tris, or 0.01 M PBS to achieve pH values of 5.2, 6.5, and 7.4, respectively (sections 2.3 and 2.5). Results showed that for both derivatives, it was possible to measure an auto-correlation function at all pHs, indicating the formation of self-assembled structures. The general trend was similar for both peptides (Fig. 1 A-D), but the auto-correlation functions of the WT derivative were noisier, mostly at higher pHs due to a lower scattering intensity, probably due to a lower volume fraction of assemblies (Fig. 1A). At the lowest pH, both derivatives showed a marked tendency to form larger assemblies, as shown by both auto-correlation functions and intensity-weighted size distributions (Fig. 1 A-D, red lines). This is due to the increased hydrophobicity of the peptides in acidic conditions, where their net charge is diminished. As a result, the reduced electrostatic repulsion among peptide molecules facilitates aggregation. This trend was less evident for the FL-derivative (Fig. 1 C-D), suggesting that the conjugation with FL affects the peptide self-assembling behavior. Investigations into the colloidal stability of pHLIP dispersions over time revealed that their stability at physiological pH was preserved for at least 24 h (Figure S2 A-B and G-H). Similar stability was observed for FL-pHLIP under slightly acidic conditions (pH 6.5) (Figure S2 I-L). However, at highly acidic pH levels, aggregation was noted, leading to the formation of micrometer-sized particles (Figure S2 M-N). Considering that intraoperative fluorescence imaging requires peptide stability over the surgical timeframe ($\leq$ 6 h), the 24 h colloidal stability observed for WT- and FL-pHLIP (Figure S2) is fully sufficient for the intended application.

Table 1
Experimental conditions for WT- pHLIP solubility evaluation.

[pHLIP] (mM)	Treatment procedures			Appearance	Solubility/ dispersibility
	Vortex	**Sonication**	**Heating**		
2.5	✓	X	X	Totally insoluble	Absent
1.2	✓	X	X	Presence of lumps	Poor
0.8	✓	✓	X	Homogeneous, opaque	Medium
0.6	✓	✓	✓	Homogeneous, transparent	Good

3.2. *Peptide folding, membrane interactions, and kinetics in liposome-based models of eukaryotic cells*

The mechanism of action for pHLIPs is well understood [33]. In acidic environments, protonation and increased hydrophobicity trigger the folding of the peptide into membranes. This process facilitates the selective interaction of pHLIPs with cancer cell membranes, enhancing their utility in targeted imaging and therapeutic applications [34–36]. Protonatable residues in the hydrophobic central and C-terminal regions are negatively charged at physiological pH, but neutralized at lower pH, allowing membrane integration and forming a transmembrane helix. Consequently, the pH-dependent conformational transition of the peptide within the TME underlies its ability to insert into membranes. After studying the self-assembly behavior of pHLIP derivatives in an acidic environment, we evaluated their ability to be integrated in cellular membranes using DOPC liposomes as simple model systems by circular dichroism (CD) spectroscopy.

Specifically, we started with an extensive characterization of the WT-pHLIP, using it as a control to assess the effective integration of FL-pHLIP into the outer leaflet of lipid bilayers.

We validated the published data on the CD membrane-insertion profile of WT-pHLIP, which retained a random coil secondary structure at physiological pH in the presence of DOPC liposomes, suggesting minimal interaction with the liposomes (Fig. 2A, state II, dark line) [37]. Conversely, the CD pattern began to change at slightly acidic pH, reaching a clear α-helix profile at pH 5.2, characterized by a double minimum at 208 and 222 nm (Fig. 2A, state III, green and red lines). FL conjugation did not affect the membrane insertion properties of the peptide. Indeed, FL-pHLIP showed a random coil secondary structure at physiological pH, which progressively changed into an α-helix conformation upon lowering the pH (Fig. 2B). After confirming that FL-pHLIP mirrors the behavior of the WT peptide, we shifted our focus solely to the FL-containing derivative, which is the desired probe for imaging applications.

To investigate the kinetics of FL-pHLIP membrane insertion, CD analyses were performed in acidic conditions (pHs equal to 5.2 and 6.5; see Figs. 3A and 3B) at specified time intervals (5, 20, 50, and 70 min). A mild acidic pH (6.5–6.8) is included in our experimental design, as it represents the typical conditions found in GB tumors [38].

Peptide folding occurred almost instantly, as evidenced by the detectable α-helix formation at 5 min, even at mild acidic pH (Fig. 3B). After FL-pHLIP was incorporated into the lipid bilayer, its secondary structure remained stable over time, indicating that the peptide is firmly anchored to the membrane. These findings suggest that membrane insertion at acidic pH occurs quickly and remains stable.

3.2.1. *Quantification of the inserted peptide into the lipid bilayer*

A semi-quantitative evaluation of the embedded FL-pHLIP in the lipid membrane as a function of pH and time was performed using unilamellar DOPC liposomes. After mixing FL-pHLIP with DOPC liposomes (see Content S4 of the Supplementary Material), the liposomes were separated from free peptide using gel permeation chromatography (GPC, Sephadex G-25, Fig. 4A). The isolated liposomes were then characterized by DLS and UV-Vis spectroscopy. Specifically, DLS data on the purified samples indicated an increase in liposome hydrodynamic size (keeping constant the PDI) with decreasing pH, indicating an increasing peptide integration into the lipid membrane with modification of the liposome's surface properties and hydration sphere (Figs. 4B-C). Although fluorescein works as a pH sensor with a decreased absorbance in acidic environments, as demonstrated in our additional studies on FL salt (S3 A-B), the UV-Vis analysis of the purified samples showed a higher FL-pHLIP intensity at λ_{max} (450–500 nm) at acidic pH values

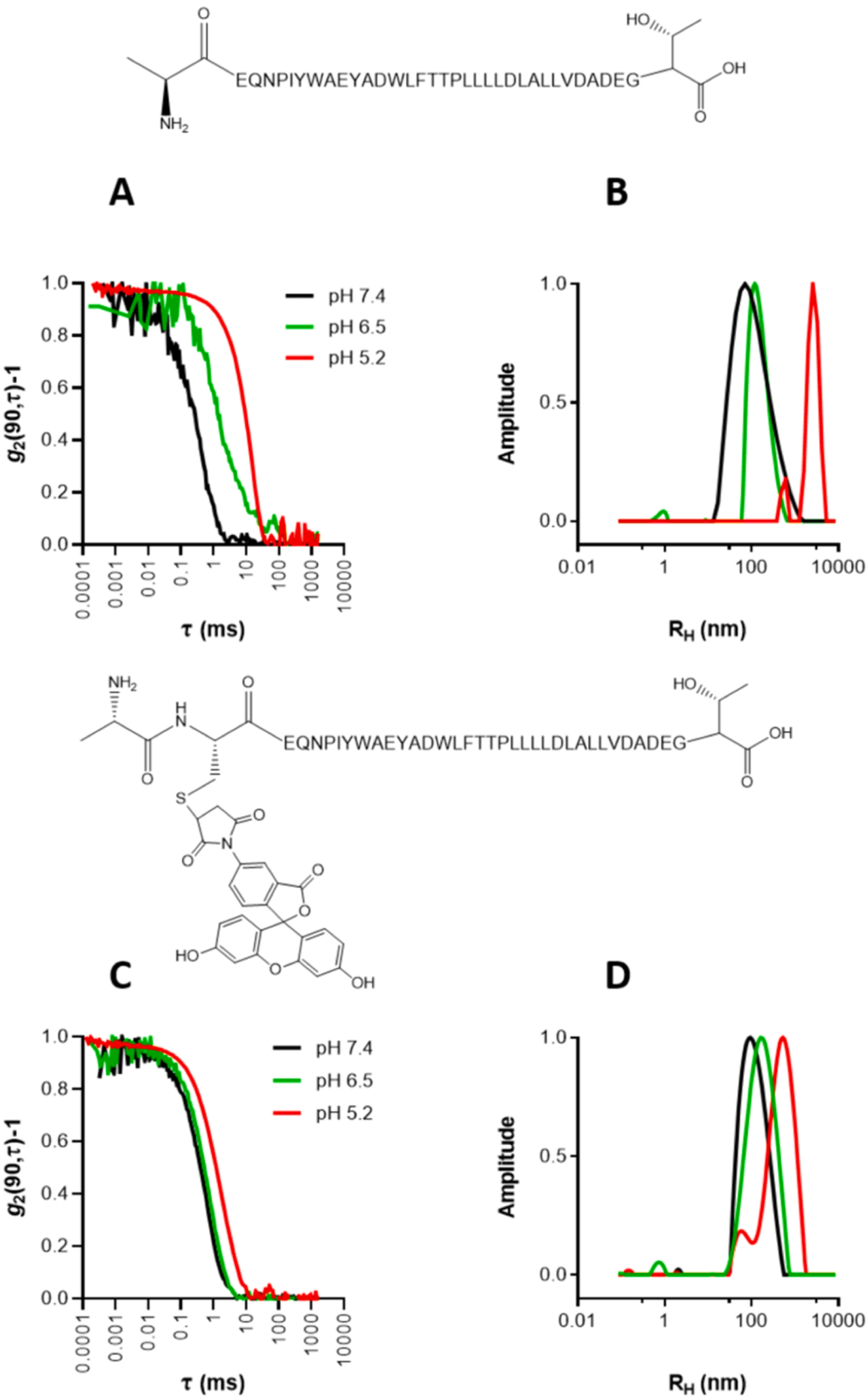

Fig. 1. Self-assembly properties of pHLIP peptides in physiological and acidic environments. Dynamic Light Scattering (DLS) measurements at $\theta = 90^\circ$ of WT (A-B) and FL-pHLIP (C-D) peptides in solutions at pH 7.4, 6.5, and 5.2 (black, green, and red lines, respectively). Panels A and C display the DLS autocorrelation functions for the two samples (A, C). The corresponding intensity-weighted size distributions (B, D) (radius, $<R_H>$, nm) are shown in panels B and D.

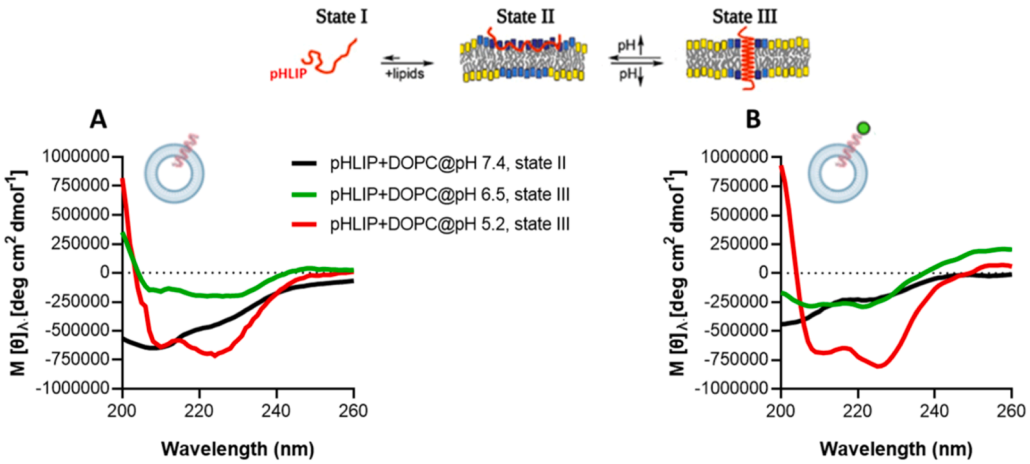

Fig. 2. Peptide structuring and membrane insertion properties. Transitions between distinct states of WT (A) and FL pHLIPs (B) in the presence of DOPC liposomes were monitored using Circular Dichroism (CD) spectroscopy. At pH 7.4, peptides remained in state II, while exposure to acidic pH conditions (state III: pH 6.5 and 5.2, represented by green and red lines, respectively) induced specific structural changes.

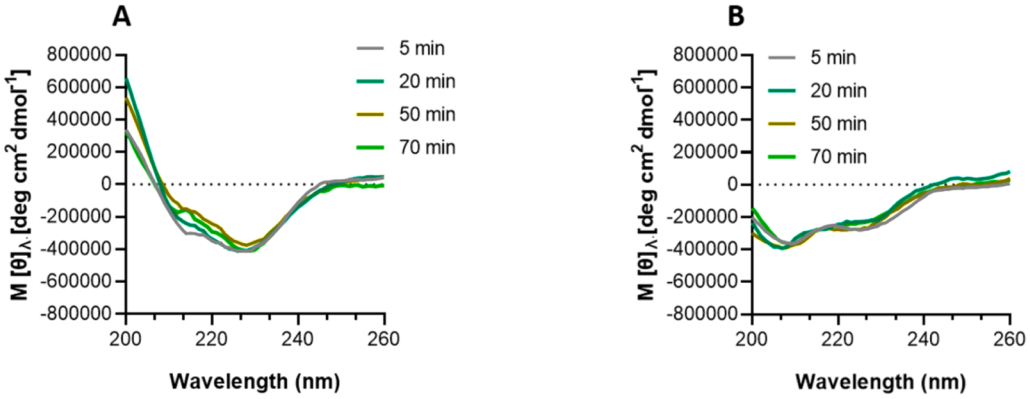

Fig. 3. FL-PHLIP membrane insertion at acidic pH values over time. Representative Circular Dichroism (CD) spectroscopy profiles illustrating the kinetics of peptide-membrane interactions in the presence of DOPC liposomes at pH 6.5 (A) and 5.2 (B).

compared to physiological conditions, where no peak was detected (Fig. 4D). This indicates that FL-pHLIP is a highly effective membrane binder at low pH, while at pH 7.4, it only weakly interacts with the lipid membranes, but it is fully removed upon purification. UV-Vis time-resolved measurements showed that peptide insertion nearly reached saturation after 30 min of incubation, particularly at mild acidic pH. Under higher acidic conditions (pH 5.2), approximately 40 % of FL-pHLIP integrated into the membrane within the first 30 min, maintaining this level for several hours and ultimately reaching a maximum of 57 % after 24 h (Figure S5).

3.3. *pHLIP-membrane integration on SLB surfaces*

In the second part of the study, we employed supported DOPC lipid bilayers (SLBs) as a simplified model to assess the sensitivity of pHLIP derivatives in a cell membrane environment. Although other systems as micron-sized liposomes, have recently been proposed as biomimetic models due to their native-like membrane curvature [39–41], their limited mechanical stability and short lifetime constrain their applicability in extended or flow-based assays. By contrast, SLBs offer enhanced robustness, compatibility with advanced surface characterization techniques [42]. In our experiments, the interaction between pHLIP and SLBs was monitored by QCM-D and confocal fluorescent microscopy. Historically, SLB platforms have been widely exploited for peptide functionalization to investigate cellular properties such as adhesion, growth, and differentiation [43–46], and SLBs combined with QCM-D have proven effective for studying peptide binding, distinguishing mechanisms of action, and assessing membrane integrity [47–50]. Here, we aimed to evaluate the insertion efficiency.

3.3.1. *In-Flow model of eukaryotic cell membranes: QCM-D*

QCM-d experiments were performed to evaluate pHLIP binding efficiency at different pHs by calculating mass and structural changes of the lipid membrane upon pHLIP incubation [51]. The detailed configuration of the QCM experimental setup is provided in Content S6 of the Supplementary Material and in Section 2.9 of the *Methods*. We investigated the interaction of FL-pHLIPs with DOPC membranes using a peptide concentration of 0.5 μM, based on the pHLIPs concentration range typically used for cellular applications [35,37,52]. We first optimized a method to obtain a stable lipid bilayer in the QCM-d chip, starting from the introduction of a DOPC liposome dispersion into the QCM-D chamber. The accomplishment of values of – 25 Hz and about 0 for Δf and ΔD, respectively, indicates the successful formation of a complete bilayer, which remained stable during subsequent washing with the incubation buffer over time (see Figures S7 A-C in Supplementary Material and Section 2.9 of the *Methods*). This system served as the reference system (sequence 1–2–1–3–1 in Figs. 5 A-C). The introduction of FL-pHLIP dispersion at physiological pH (arrow 4 in Fig. 5A) was followed by a slight decrease in frequency, suggesting a mild and temporary peptide-lipid bilayer interaction. Indeed, during static incubation and subsequent washing with PBS, the frequency decreased and reverted to its original value, indicating a full washing of the adsorbed

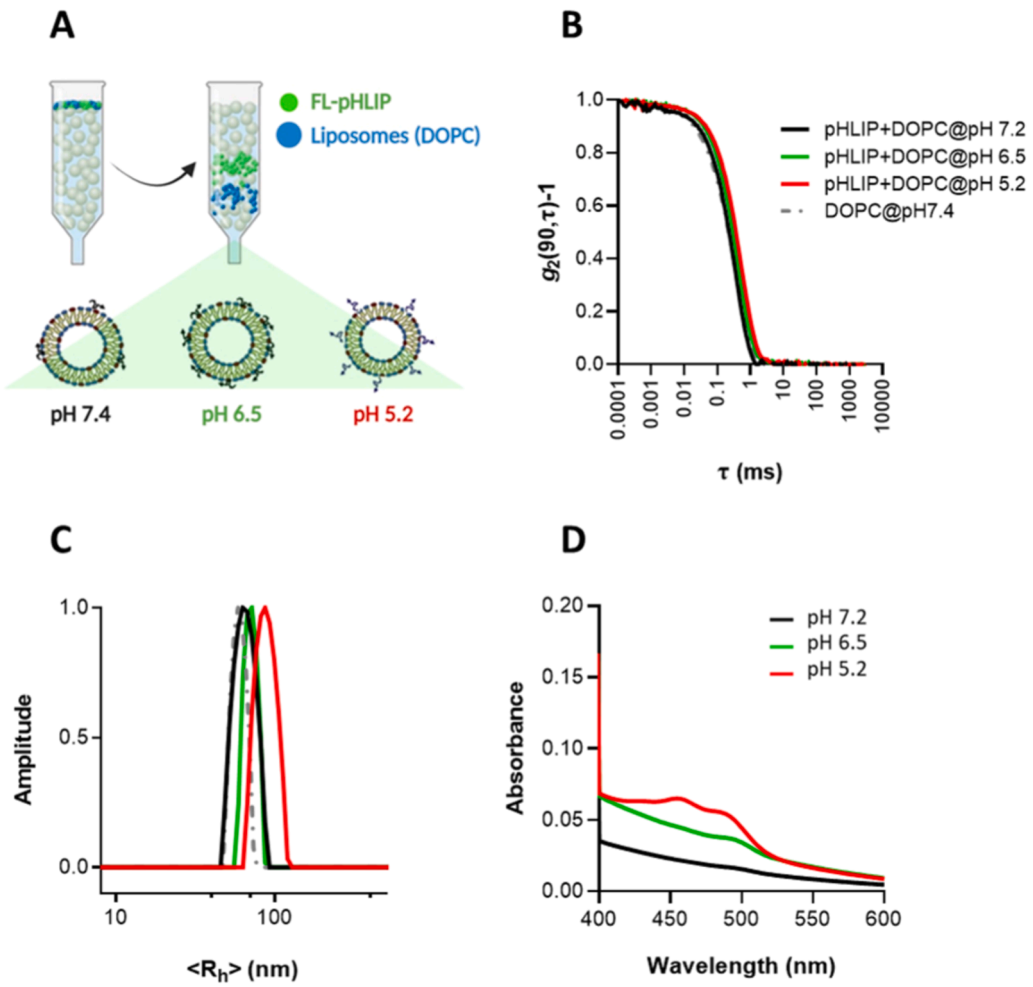

Fig. 4. Quantification of the inserted peptide into the lipid bilayer. (A) Schematic representation of the peptide purification process after interaction with DOPC liposomes, using the Sephadex-25 gel filtration method. After a 2-hour interaction with liposomes, non-inserted peptides were removed, and pHLIP-associated liposomes were characterized using Dynamic Light Scattering (DLS) measurements. Auto-correlation functions of untreated and pHLIP-associated DOPC liposomes as a function of pH (B) and corresponding intensity-weighted size distributions (C). UV–vis analyses of DOPC and pHLIP mixtures at different pH levels after Sephadex purification to evaluate pHLIP insertion into the lipid membrane (D).

peptide. Conversely, at lower pH levels (i.e., pH=6.5 and 5.2, Fig. 5B-C), we observed a rapid increase in dissipation and a decrease in frequency immediately after the peptide flow. The reached values remained unchanged during the final buffer wash, confirming a strong insertion of the peptide in the lipid membrane. We could also evaluate the mass deposition upon pHLIP flow on the chip, which resulted in higher amounts at more acidic pH levels (Fig. 5D; 633 ± 18 and 2258 ± 980 ng/cm^2 for pH 6.8 and 5.2, respectively). In both cases, the similarity in the resonance frequency across distinct harmonics indicates that mass density is uniform throughout the entire thickness [51] of the membrane, as previously demonstrated for cell-penetrating peptides [53]. Although the peptide insertion is highly stable, it is reversible. Indeed, if the final wash is conducted in a non-acidic pH environment, the inserted mass is lost, and both Δf and ΔD return to the characteristic values of only SLB, suggesting that it is not altered by peptide binding (Figure S8).

3.3.2. *Confocal analysis of pHLIP-interacting SLBs*

The peptide-membrane interaction was further investigated through confocal microscopy. For this purpose, the same DOPC SLB used in QCM studies was tagged with a fluorescent dye (Cy5, Sulfo-Cyanine5, shown in blue in Fig. 6 A-L) and imaged after treatment with the FL-pHLIP. Axial acquisitions, corresponding to an inner section of the bilayer (Fig. 6 A-C and F-H), measured before and after buffer washing, confirmed that at pH 7.4, the observed FL fluorescence (green) was fully removed after washing. This means that the fluorescence was primarily due to free peptide in solution (green, Fig. 6E), as it was completely removed after washing with the incubation buffer, leaving only the blue SLB detectable (Fig. 6H and L). At pH ≤ 6.5, the SLB retained bright green fluorescent spots (homogeneously distributed within the membrane, Fig. 6 A-B and D) even after buffer washing (Fig. 6 F-G and I). The 3D reconstruction of the rinsed SLB after incubation with the pHLIP peptide at both physiological and highly acidic pH levels further supported this conclusion (Figure S9 A-B).

To demonstrate the reversibility of the peptide-membrane interaction, we incubated the SLB with FL-pHLIP at a slightly acidic pH (Fig. 7A) and subsequently washed it with a buffer at physiological pH (Fig. 7B). This washing procedure completely removed all of the inserted peptide, corroborating our previously reported QCM data.

The same experimental setup was finally extended to a scrambled peptide (SC-FL pHLIP), which is not pH-sensitive, and used as a control. Results showed that SC-FL pHLIP showed the same affinity for the lipid bilayer regardless of pH (Figure S10 A-C, **D-E and S11 A-B**). Furthermore, the fluorescence of the peptide showed a different appearance compared to FL-pHLIPs. Indeed, we observed larger spots within the membrane, potentially due to peptide instability and aggregation. The insertion appeared to be stable, as the SLB maintained an analogous appearance after washing at the same pH conditions, with a persistent presence of the peptide (Figure S10 F-H and I-L). Together, these results

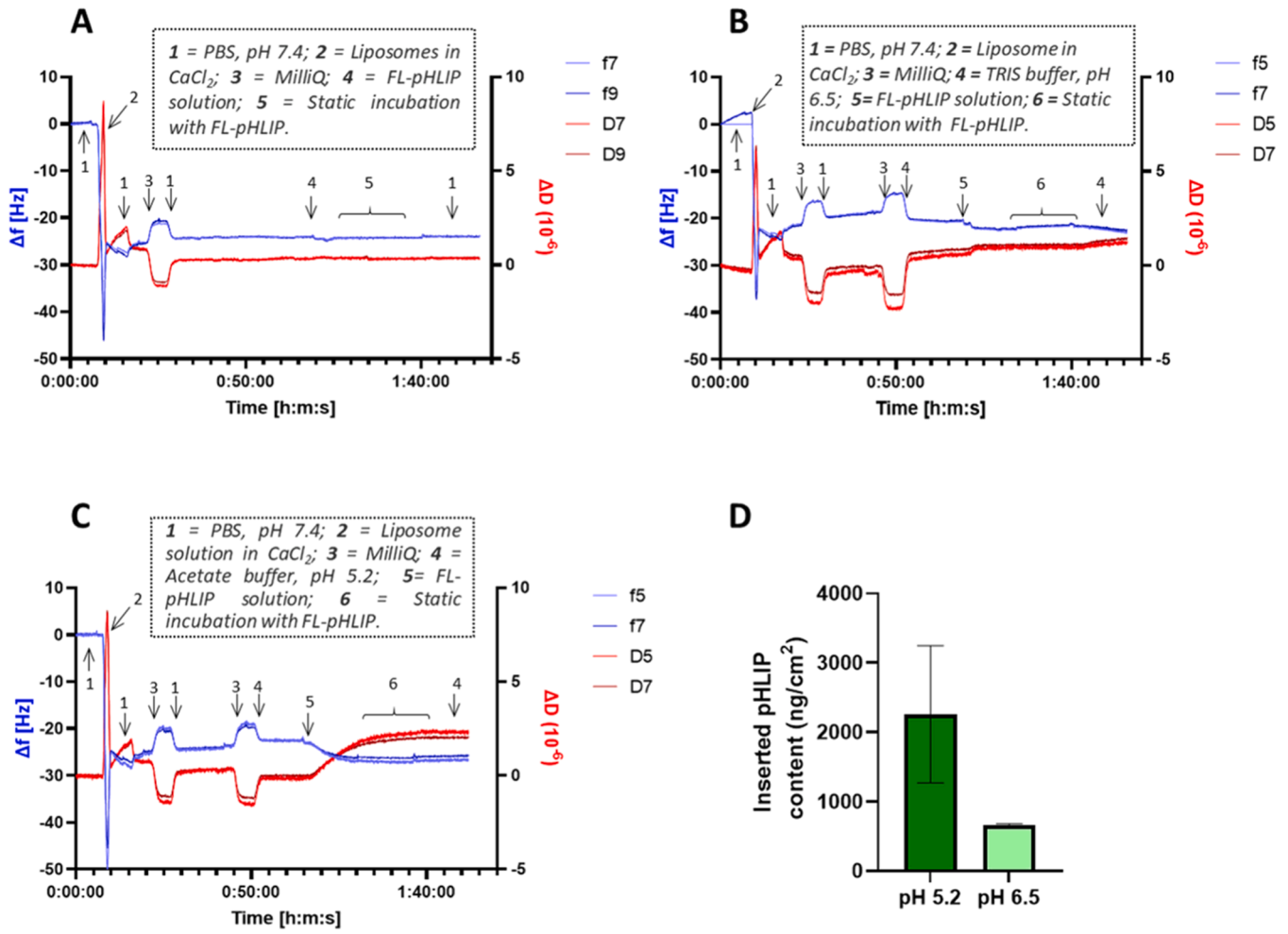

Fig. 5. In-Flow model of eukaryotic cell membranes: QCM-D experiments. Δf–t and ΔD–t plots are shown in a representative QCM-D measurement, illustrating the SLB response after FL-pHLIP incubation at pH 7.4 (A), pH 6.5 (B), and pH 5.2 (C). (D) Quantification of FL-pHLIP insertion into the SLB at acidic pH values (5.2 and 6.5).

demonstrate the unique performance and sensitivity of the proposed FL-pHLIP sequence.

3.4. Binding efficacy of FL-pHLIP on primary cell lines from newly diagnosed glioblastoma

The final part of this study focuses on the cellular validation of FL-pHLIP binding efficacy in different patient-derived GB primary cells. Representative primary cell lines growing *in vitro* as neurospheres (glioblastoma GB-NS) were analyzed across all molecular subtypes (proliferative/classical, mesenchymal, or proneural), derived from both newly-diagnosed (ND) and recurrent glioblastomas (R). Cells were cultured at different pHs (*i.e.,* 7.4 and 6.5). Indeed, since FL-pHLIP targets the acidic extracellular pH characteristic of the GB microenvironment rather than a tumor-specific membrane marker, the physiologic pH of healthy tissues (pH 7.4) represents the proper negative control. In a preliminary set of experiments, the most efficient FL-pHLIP concentration for incubation was determined. A specific range of peptide concentrations was selected (0.5–10 μM) [37,52,54], and cells were incubated for 2 h at both pH levels. In addition, the scrambled version of pHLIP, SC-FL pHLIP, was used as a pH-insensitive control. No cytotoxicity was observed for any of the tested concentrations of either peptide (Figure S12 A). Binding efficiency, quantified by flow cytometry, indicated a membrane affinity independent of pH for SC-FL pHLIP (cell positivity to fluorescein, Figure S12 B), with even greater efficiency observed at physiological pH. In contrast, FL-pHLIP showed significantly increased cell positivity at slightly acidic compared to physiological pH (Figure S12 C). This effect was particularly evident at lower concentrations, while higher concentrations (e.g., 10 μM) exhibited reduced efficiency and a less significant difference in pH-dependent response.

Moreover, in this setting, cell labeling at physiological pH was minimal, effectively reducing non-specific targeting (Figure S12 C). These findings indicate that a mild concentration of FL-pHLIP (5 μM) is more appropriate for our objectives and was chosen for further, more detailed cellular assays.

We then tested the pH-sensitive system on newly-diagnosed and recurrent glioblastoma primary cell lines derived from the same patients. Both GB-NS lines were incubated with FL-pHLIP using the experimental conditions optimized before. As expected, cells well tolerated both ctrl and FL-pHLIP peptides (Fig. 8 A, B). GB-NS from ND or R specimens showed the same behavior (Fig. 8 A, C, and B, D respectively). Specifically, both peptides demonstrated a certain affinity for the cellular membrane even at physiological pH, due to the hydrophobic residues. However, while SC-FL showed the same affinity at both pH levels, FL-pHLIP confirmed a strongly increased efficiency at pH 6.5 compared to pH 7.4 (Fig. 8 B and D, respectively). The inclusion of paired ND and R specimens from the same patients, together with distinct tumor phenotypes (Figure S12), provided a rigorous control and highlighted the specificity and versatility of the system across different TME contexts.

With confocal microscopy on the same recurrent GB-NS, we first confirmed the pH-dependent enhanced performance of FL-pHLIP

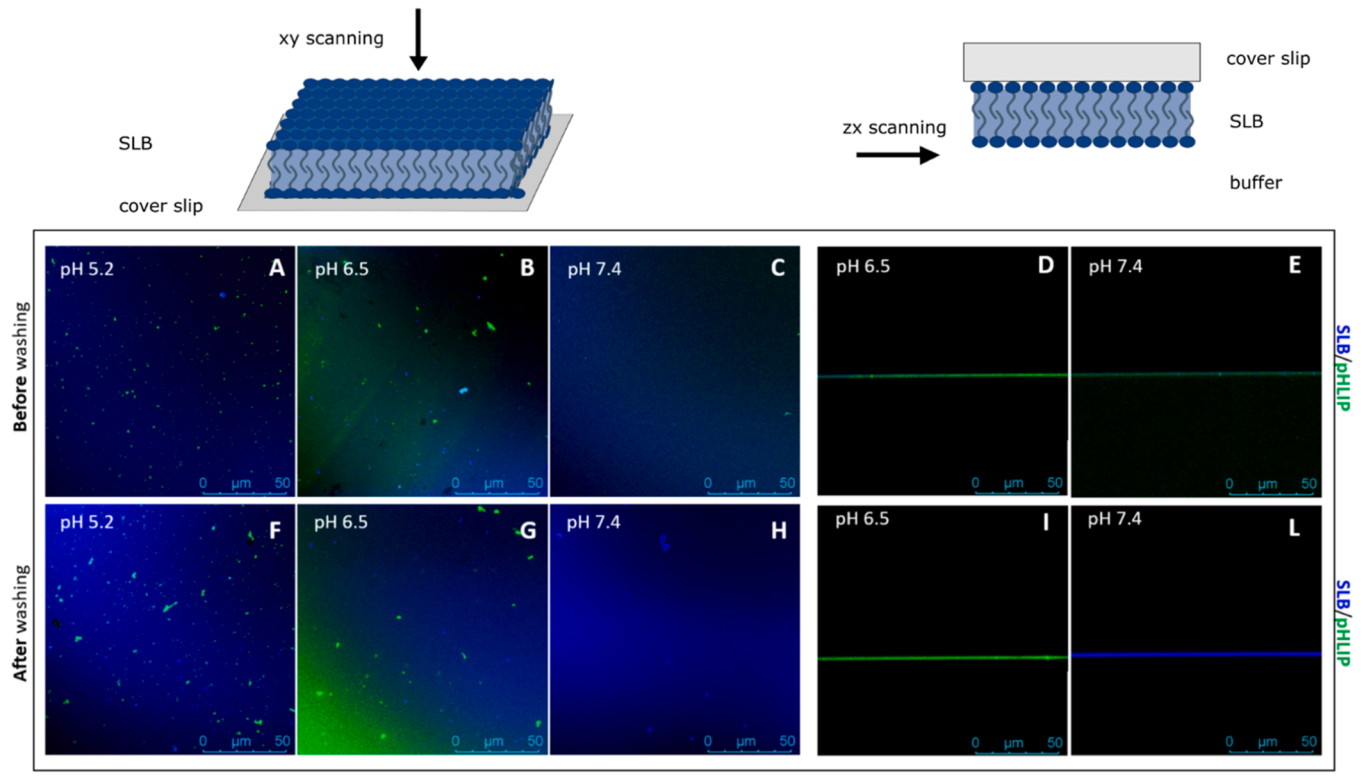

Fig. 6. Confocal analysis of pHLIP-interacting SLBs. Representative fluorescence images of DOPC SLB (blue) after a 30-minute incubation with FL-pHLIP (green) at different pH levels, both before (A-E) and after (F-L) a washing process using the same buffer and pH conditions as during peptide incubation. The images display axial (A-C, F-H) and sagittal sections of the DOPC SLB interacting with pHLIP (D-E and I-L).

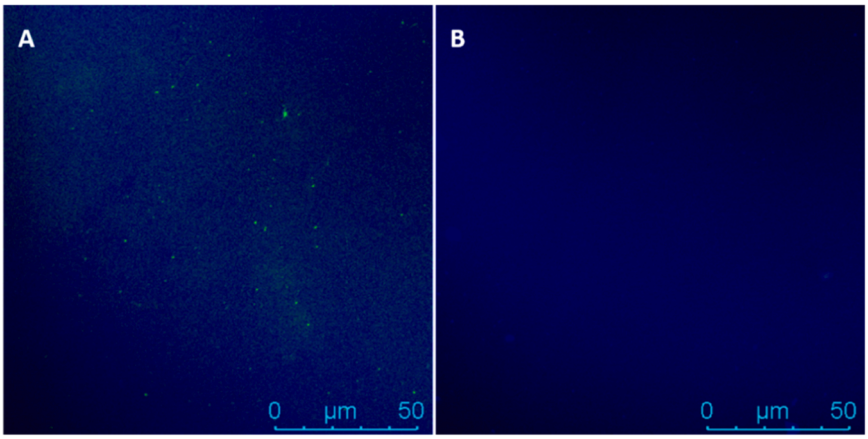

Fig. 7. Study of reversibility of the peptide-membrane interaction by confocal analysis of SLB. Axial sections of DOPC SLB interacting with pHLIP at acidic (A), following a wash with buffer at pH 7.4 (B).

(green), as indicated by more abundant and intense green dots at acidic pH (Fig. 9 F versus Fig. 9 P). Notably, we verified the membrane insertion of the peptide, as demonstrated by the co-localization of pHLIP with B7-H3, a transmembrane protein overexpressed in GB [55] (Fig. 9 R). All these results together demonstrated the optimal efficiency of FL-pHLIP in a representative and heterogeneous GB-associated context, supporting its translation first to *in vivo* GB animal models, and ultimately to clinical applications.

4. Conclusions

In this study, we developed and characterized a novel fluorescein-conjugated pH-sensitive peptide (FL-pHLIP) for GB imaging, with the intention of enhancing fluorescence-guided GB resection surgery. Rather than designing a new sequence, we repurposed the well-established pHLIP scaffold, exploiting its proven responsiveness to extracellular acidity in a pathological context of urgent clinical need. Precise intraoperative identification of GB margins remains critical, as surgery is still the only effective therapeutic option for this incurable disease. While previous research has primarily concentrated on conjugating pHLIP derivatives with near-infrared (NIR) dyes [56], we linked the peptide to fluorescein (FL) to generate a tracer compatible with standard neurosurgical workflows. This approach aimed to meet the medical needs associated with the microsurgical resection of GB in preparation for clinical development, such as being detectable using conventional surgical microscopes and being administered

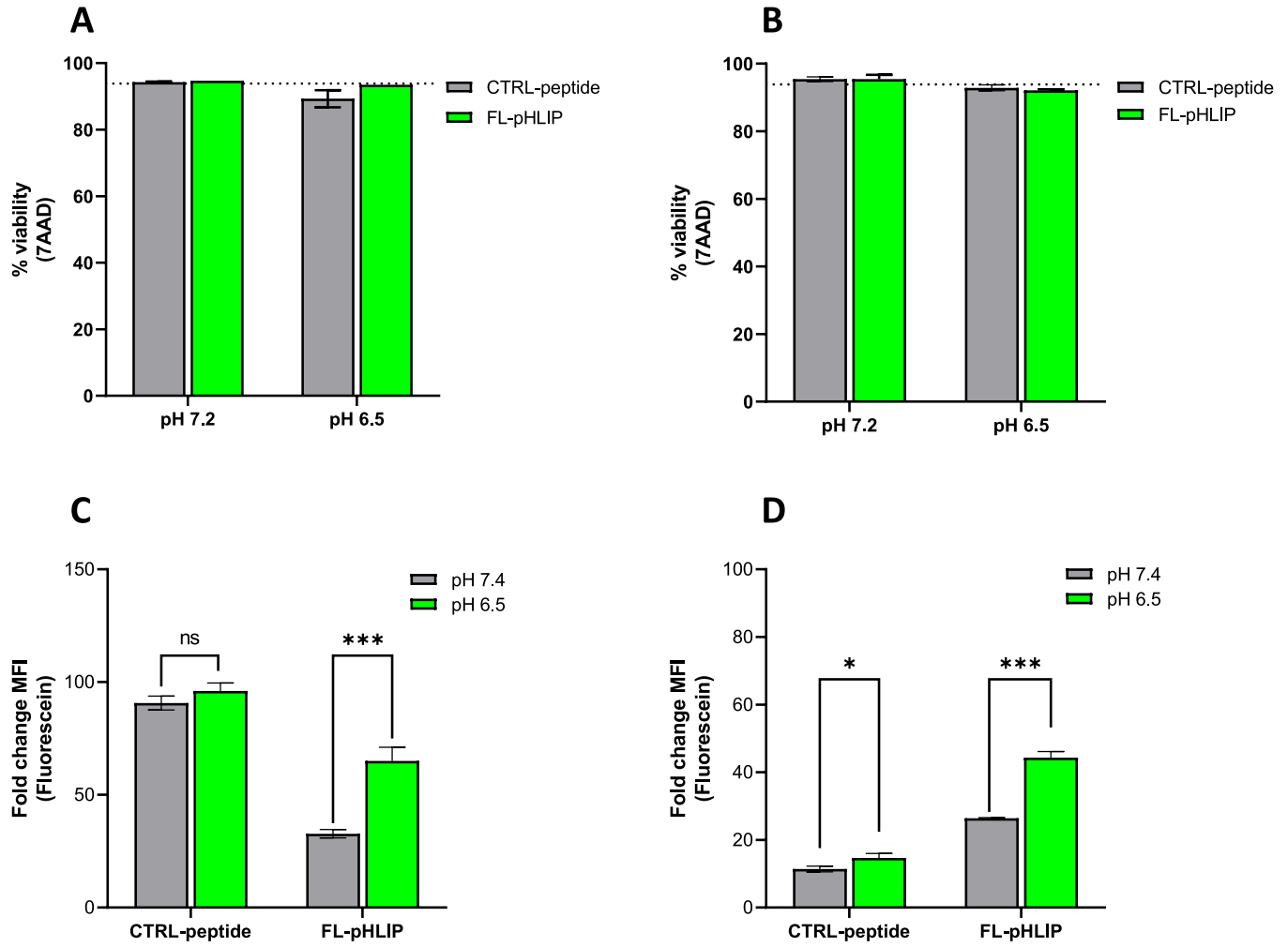

Fig. 8. *In vitro* experiments on primary human GB cells. Cell tolerance to both scrambled (gray) and FL-pHLIP (green) was assessed in primary surgeries (A) and recurrent (B) GB cells. Peptide binding efficiency was quantified using flow cytometry, measuring cell positivity for fluorescein (expressed as fold change in mean fluorescence index, MFI) in both cell lines (C: primary surgery, D: recurrence). The reported values represent the mean ± standard deviation, based on a minimum of n = 3 biological replicates per condition. Each experiment was performed at least twice.

simultaneously during surgery. Although FL possesses a fluorescence quantum yield that decreases at acidic pH, our experiments have primarily demonstrated that even in the mildly acidic conditions typical of GB, the strong selectivity of the tracer for lipid membranes resulted in a more intense signal than in physiological conditions at pH 7.4. This indicates that, despite the variations in fluorescence yield of the dye related to pH, our tracer maintains its effectiveness and utility in practical applications. Furthermore, while previous studies on pHLIP derivatives, beyond testing their biological efficacy, were limited to investigating peptide folding mechanisms as a function of the pH using liposomes [36,37,57], we took a more nuanced approach. We performed time-response QCM-d and confocal microscopy experiments to study the binding mechanism and fluorescence response of the FL-pHLIP derivative with SLBs, mimicking the cellular membrane, as a function of time and pH. Importantly, the screening of non-pH-responsive scrambled peptides revealed a membrane affinity that remained unaffected by changes in pH, confirming the selectivity of the developed tracer.

Overall, we developed a tiered methodology first studying the interaction mechanism of FL-PHLIP with lipid membrane models (liposomes and supported lipid bilayers) and validating their selectivity on patient-derived cell lines. This approach will significantly accelerate the future screening of next-generation peptides with similar properties and potential therapeutic applications, specifically in assessing their selectivity and binding efficiency at relevant pH levels and in biological environments associated with GB.

Notably, similar methodologies have been used to study the interactions of pH-responsive cell-penetrating and anti-microbial peptides with lipid membranes [48,49,58,59], primarily focusing on the mechanisms of membrane disruption that lead to cell death and guiding the development of new antibiotics. However, unlike these studies, which aim to understand how membranes are compromised, our study focuses on ensuring the robustness of the binding, its kinetics and efficiency even at a weakly acidic pH without alteration of the lipid bilayer.

Finally, the experiments on primary GB cells in heterogeneous conditions, including first-line interventions, recurrences, and varying metabolic classifications, validated the tracer's performance in diverse biological environments. These findings confirm that its targeting mechanism is conserved across diverse membrane environments and phenotypes, supporting its translational potential. *In vivo* testing is currently planned to validate our results and potentially pave the way for clinical applications. Overall, our findings establish a strong foundation for significantly improving the intraoperative identification of glioblastoma tissue, which could have a profound impact on patient survival.

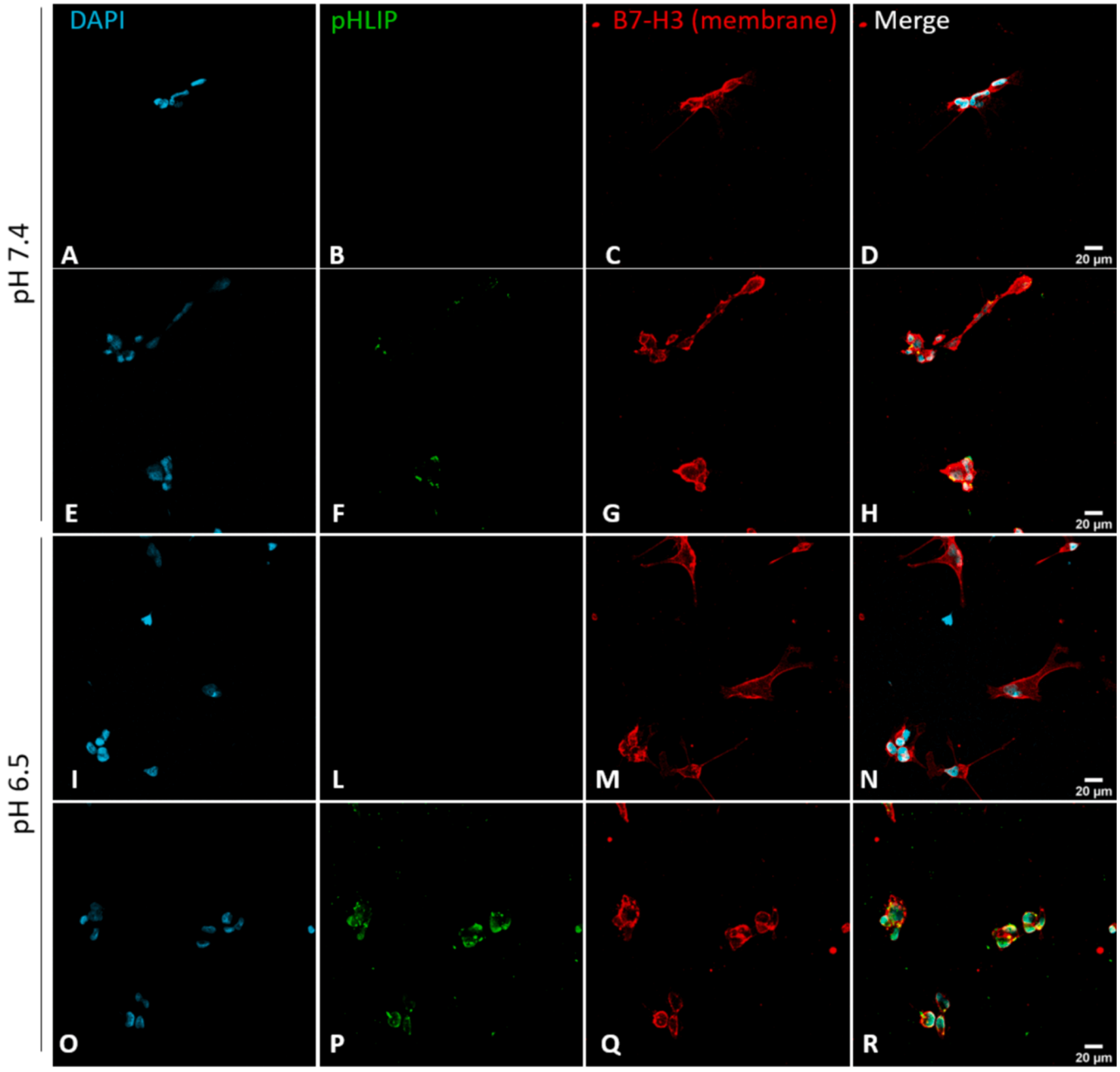

Fig. 9. Confocal microscopy analysis of recurrent GB cells, both untreated (no peptide exposure; A-D and I-N) and following interaction with FL-pHLIP (E-H and O-R) at physiological and slightly acidic conditions (pH 7.4 and 6.5, respectively). Cells were stained to visualize nuclei (DAPI, light blue) and cellular membranes (B7H3 transmembrane protein, red), facilitating the pHLIP localization of FL-pHLIP (green) insertion into GB cells under acidic conditions. Images were captured at 40X magnification.

CRediT authorship contribution statement

Cristina Chirizzi: Writing – review & editing, Writing – original draft, Visualization, Methodology, Investigation, Conceptualization. **Serena Pellegatta:** Writing – review & editing, Writing – original draft, Supervision, Methodology, Funding acquisition, Conceptualization. **Francesca Baldelli Bombelli:** Writing – review & editing, Writing – original draft, Supervision, Methodology, Funding acquisition. **Alessandro Gori:** Writing – review & editing, Writing – original draft, Supervision, Methodology, Funding acquisition, Conceptualization. **Marina Grisoli:** Writing – review & editing. **Francesco Acerbi:** Writing – review & editing, Methodology, Conceptualization. **Martina Beccalli:** Writing – review & editing, Methodology, Investigation. **Arianna Balestri:** Writing – review & editing, Visualization, Methodology, Investigation. **Costanza Montis:** Writing – review & editing, Methodology. **Martina Maffezzini:** Writing – review & editing, Visualization, Methodology, Investigation. **Nadia Mosca:** Writing – review & editing, Visualization, Methodology, Investigation.

Funding sources

This study was partially supported by the CALabria HUB for Innovative and Advanced Research - CALHUB.RIA, specifically the "Creation of Life Sciences Hubs" project T4-AN-09, program ZRPOS2, and partially by the Italian Ministry of Health (RRC - Current Research 2022–2024).

Declaration of Competing Interest

The authors declare that they have no known competing financial interests or personal relationships that could have appeared to influence the work reported in this paper.

Acknowledgments

The authors acknowledge the support of Brainy Associazione per la ricerca sui tumori cerebrali (Italian Association for Brain Cancer Research, Onlus). We thank Dr. Daniele Cartelli for his support in the acquisition of confocal images, the Besta Brain Tumor Biobank (BBTB), and Mr Piero Tieni (SOL Group Spa, Italy) for the cryomanagement service and the technical assistance. FBB and MB acknowledge the project Lancelot (PRIN 2022 PNRR n P2022RBF5P) funded by MUR (European Union–Next Generation EU).

Appendix A. Supporting information

Supplementary data associated with this article can be found in the online version at doi:10.1016/j.colsurfb.2025.115398.

Data Availability

Data will be made available on request.

References

[1] J. Höhne, K.M. Schebesch, C. de Laurentis, M.O. Akçakaya, C.B. Pedersen, A. Brawanski, F.R. Poulsen, T. Kiris, C. Cavallo, M. Broggi, P. Ferroli, F. Acerbi, Fluorescein sodium in the surgical treatment of recurrent glioblastoma multiforme, World Neurosurg. 125 (2019), https://doi.org/10.1016/j.wneu.2019.01.024.

[2] O. Netufo, K. Connor, L.P. Shiels, K.J. Sweeney, D. Wu, D.F. O'shea, A.T. Byrne, I. S. Miller, Refining glioblastoma surgery through the use of intra-operative fluorescence imaging agents, Pharmaceuticals 15 (2022), https://doi.org/10.3390/ph15050550.

[3] A.A. Pandith, I. Qasim, W. Zahoor, P. Shah, A.R. Bhat, D. Sanadhya, Z.A. Shah, N. A. Naikoo, Concordant association validates MGMT methylation and protein expression as favorable prognostic factors in glioma patients on alkylating chemotherapy (Temozolomide), Sci. Rep. 8 (2018), https://doi.org/10.1038/s41598-018-25169-2.

[4] A.I. Hashim, X. Zhang, J.W. Wojtkowiak, G.V. Martinez, R.J. Gillies, Imaging pH and metastasis, NMR Biomed. 24 (2011), https://doi.org/10.1002/nbm.1644.

[5] P. Sharma, A. Aaroe, J. Liang, V.K. Puduvalli, Tumor microenvironment in glioblastoma: Current and emerging concepts, NeuroOncol. Adv. 5 (2023), https://doi.org/10.1093/noajnl/vdad009.

[6] M. Alibolandi, K. Abnous, M. Ramezani, H. Hosseinkhani, F. Hadizadeh, Synthesis of AS1411-aptamer-conjugated CdTe quantum dots with high fluorescence strength for probe labeling tumor cells, J. Fluoresc. 24 (2014), https://doi.org/10.1007/s10895-014-1437-5.

[7] M. Alibolandi, K. Abnous, F. Sadeghi, H. Hosseinkhani, M. Ramezani, F. Hadizadeh, Folate receptor-targeted multimodal polymersomes for delivery of quantum dots and doxorubicin to breast adenocarcinoma: In vitro and in vivo evaluation, Int. J. Pharm. 500 (2016), https://doi.org/10.1016/j.ijpharm.2016.01.040.

[8] W. He, H. Hosseinkhani, R. Mohammadinejad, Z. Roveimiab, D.Y. Hueng, K.L. Ou, A.J. Domb, Polymeric nanoparticles for therapy and imaging, Polym. Adv. Technol. 25 (2014), https://doi.org/10.1002/pat.3381.

[9] R.S. Sarabi, E. Sadeghi, H. Hosseinkhani, M. Mahmoudi, M. Kalantari, M. Adeli, Polyrotaxane capped quantum dots as new candidates for cancer diagnosis and therapy, J. Nanostruct. Polym. Nanocompos. 7 (2011).

[10] X. Wu, Y. Xin, H. Zhang, L. Quan, Q. Ao, Biopolymer-based nanomedicine for cancer therapy: opportunities and challenges, Int. J. Nanomed. Volume 19 (2024) 7415–7471, https://doi.org/10.2147/IJN.S460047.

[11] O.A. Andreev, D.M. Engelman, Y.K. Reshetnyak, PH-sensitive membrane peptides (pHLIPs) as a novel class of delivery agents, Mol. Membr. Biol. 27 (2010), https://doi.org/10.3109/09687688.2010.509285.

[12] R.C. Adochite, A. Moshnikova, S.D. Carlin, R.A. Guerrieri, O.A. Andreev, J. S. Lewis, Y.K. Reshetnyak, Targeting breast tumors with pH (Low) insertion peptides, Mol. Pharm. 11 (2014), https://doi.org/10.1021/mp5002526.

[13] O.A. Andreev, D.M. Engelman, Y.K. Reshetnyak, Targeting diseased tissues by pHLIP insertion at low cell surface pH, Front. Physiol. 5 (2014), https://doi.org/10.3389/fphys.2014.00097 (MAR).

[14] C.J. Cheng, R. Bahal, I.A. Babar, Z. Pincus, F. Barrera, C. Liu, A. Svoronos, D. T. Braddock, P.M. Glazer, D.M. Engelman, W.M. Saltzman, F.J. Slack, MicroRNA silencing for cancer therapy targeted to the tumour microenvironment, Nature 518 (2015), https://doi.org/10.1038/nature13905.

[15] D. Wijesinghe, D.M. Engelman, O.A. Andreev, Y.K. Reshetnyak, Tuning a polar molecule for selective cytoplasmic delivery by a pH (Low) insertion peptide, Biochemistry 50 (2011), https://doi.org/10.1021/bi2009773.

[16] M. An, D. Wijesinghe, O.A. Andreev, Y.K. Reshetnyak, D.M. Engelman, PH-(low)-insertion-peptide (pHLIP) translocation of membrane impermeable phalloidin toxin inhibits cancer cell proliferation, Proc. Natl. Acad. Sci. USA 107 (2010), https://doi.org/10.1073/pnas.1014403107.

[17] Y.K. Reshetnyak, L. Yao, S. Zheng, S. Kuznetsov, D.M. Engelman, O.A. Andreev, Measuring tumor aggressiveness and targeting metastatic lesions with fluorescent pHLIP, Mol. Imaging Biol. 13 (2011), https://doi.org/10.1007/s11307-010-0457-z.

[18] S. MacHoll, M.S. Morrison, P. Iveson, B.E. Arbo, O.A. Andreev, Y.K. Reshetnyak, D. M. Engelman, E. Johannesen, In Vivo pH imaging with 99mTc-pHLIP, Mol. Imaging Biol. 14 (2012), https://doi.org/10.1007/s11307-012-0549-z.

[19] Z. Cruz-Monserrate, C.L. Roland, D. Deng, T. Arumugam, A. Moshnikova, O. A. Andreev, Y.K. Reshetnyak, C.D. Logsdon, Targeting pancreatic ductal adenocarcinoma acidic microenvironment, Sci. Rep. 4 (2014), https://doi.org/10.1038/srep04410.

[20] T.T. Tapmeier, A. Moshnikova, J. Beech, D. Allen, P. Kinchesh, S. Smart, A. Harris, A. McIntyre, D.M. Engelman, O.A. Andreev, Y.K. Reshetnyak, R.J. Muschel, The pH low insertion peptide pHLIP variant 3 as a novel marker of acidic malignant lesions, Proc. Natl. Acad. Sci. U. S. A. 112 (2015), https://doi.org/10.1073/pnas.1509488112.

[21] T. Crawford, A. Moshnikova, S. Roles, D. Weerakkody, M. DuPont, L.M. Carter, J. Shen, D.M. Engelman, J.S. Lewis, O.A. Andreev, Y.K. Reshetnyak, pHLIP ICG for delineation of tumors and blood flow during fluorescence-guided surgery, Sci. Rep. 10 (2020), https://doi.org/10.1038/s41598-020-75443-5.

[22] D.W. Demoin, L.C. Wyatt, K.J. Edwards, D. Abdel-Atti, M. Sarparanta, J. Pourat, V. A. Longo, S.D. Carlin, D.M. Engelman, O.A. Andreev, Y.K. Reshetnyak, N. Viola-Villegas, J.S. Lewis, PET imaging of extracellular pH in tumors with 64Cu- and 18F-Labeled pHLIP peptides: a structure-activity optimization study, Bioconjug. Chem. 27 (2016), https://doi.org/10.1021/acs.bioconjchem.6b00306.

[23] C. Orillac, W. Stummer, D.A. Orringer, Fluorescence guidance and intraoperative adjuvants to maximize extent of resection, Neurosurgery 89 (2021), https://doi.org/10.1093/neuros/nyaa475.

[24] A.J. Schupper, M. Rao, N. Mohammadi, R. Baron, J.Y.K. Lee, F. Acerbi, C. G. Hadjipanayis, Fluorescence-guided surgery: a review on timing and use in brain tumor surgery, Front. Neurol. 12 (2021), https://doi.org/10.3389/fneur.2021.682151.

[25] F. Le Guern, V. Mussard, A. Gaucher, M. Rottman, D. Prim, Fluorescein derivatives as fluorescent probes for pH monitoring along recent biological applications, Int. J. Mol. Sci. 21 (2020), https://doi.org/10.3390/ijms21239217.

[26] C. Li, P.Z. Sullivan, S. Cho, M.P. Nasrallah, L. Buch, H.C. Isaac Chen, J.Y.K. Lee, Intraoperative molecular imaging with second window indocyanine green facilitates confirmation of contrast-enhancing tissue during intracranial stereotactic needle biopsy: a case series, World Neurosurg. 126 (2019), https://doi.org/10.1016/j.wneu.2019.02.231.

[27] J.Y.K. Lee, J.T. Pierce, J.P. Thawani, R. Zeh, S. Nie, M. Martinez-Lage, S. Singhal, Near-infrared fluorescent image-guided surgery for intracranial meningioma, J. Neurosurg. 128 (2018), https://doi.org/10.3171/2016.10.JNS161636.

[28] M. Mazurek, B. Kulesza, F. Stoma, J. Osuchowski, S. Mańdziuk, R. Rola, Characteristics of fluorescent intraoperative dyes helpful in gross total resection of high-grade gliomas—a systematic review, Diagnostics 10 (2020), https://doi.org/10.3390/diagnostics10121100.

[29] K.M. Schebesch, M. Proescholdt, J. Höhne, C. Hohenberger, E. Hansen, M. J. Riemenschneider, W. Ullrich, C. Doenitz, J. Schlaier, M. Lange, A. Brawanski, Sodium fluorescein-guided resection under the YELLOW 560 nm surgical microscope filter in malignant brain tumor surgery - a feasibility study, Acta Neurochir. 155 (2013), https://doi.org/10.1007/s00701-013-1643-y (Wien).

[30] N.F. Bonet, D.G. Cava, M. Vélez, Quartz crystal microbalance and atomic force microscopy to characterize mimetic systems based on supported lipids bilayer, Front. Mol. Biosci. 9 (2022), https://doi.org/10.3389/fmolb.2022.935376.

[31] G. Finocchiaro, S. Pellegatta, Immunotherapy with dendritic cells loaded with glioblastoma stem cells: from preclinical to clinical studies, Cancer Immunol. Immunother. 65 (2016) 101–109, https://doi.org/10.1007/s00262-015-1754-9.

[32] J. Behnan, B. Stangeland, T. Langella, G. Finocchiaro, W. Murrell, J.E. Brinchmann, Ultrasonic surgical aspirate is a reliable source for culturing glioblastoma stem cells, Sci. Rep. 6 (2016), https://doi.org/10.1038/srep32788.

[33] A.A. Svoronos, D.M. Engelman, Pharmacokinetic modeling reveals parameters that govern tumor targeting and delivery by a pH-Low Insertion Peptide (pHLIP), Proc. Natl. Acad. Sci. U. S. A. 118 (2021), https://doi.org/10.1073/pnas.2016605118.

[34] O.A. Andreev, A.D. Dupuy, M. Segala, S. Sandugu, D.A. Serra, C.O. Chichester, D. M. Engelman, Y.K. Reshetnyak, Mechanism and uses of a membrane peptide that targets tumors and other acidic tissues in vivo, Proc. Natl. Acad. Sci. USA 104 (2007), https://doi.org/10.1073/pnas.0702439104.

[35] M. Zoonens, Y.K. Reshetnyak, D.M. Engelman, Bilayer interactions of pHLIP, a peptide that can deliver drugs and target tumors, Biophys. J. 95 (2008), https://doi.org/10.1529/biophysj.107.124156.

[36] L.C. Wyatt, J.S. Lewis, O.A. Andreev, Y.K. Reshetnyak, D.M. Engelman, Applications of pHLIP technology for cancer imaging and therapy, Trends Biotechnol. 35 (2017), https://doi.org/10.1016/j.tibtech.2017.03.014.

[37] L.C. Wyatt, A. Moshnikova, T. Crawford, D.M. Engelman, O.A. Andreev, Y. K. Reshetnyak, Peptides of pHLIP family for targeted intracellular and extracellular delivery of cargo molecules to tumors, Proc. Natl. Acad. Sci. USA 115 (2018), https://doi.org/10.1073/pnas.1715350115.

[38] A.B. Hjelmeland, Q. Wu, J.M. Heddleston, G.S. Choudhary, J. MacSwords, J. D. Lathia, R. McLendon, D. Lindner, A. Sloan, J.N. Rich, Acidic stress promotes a glioma stem cell phenotype, Cell Death Differ. 18 (2011), https://doi.org/10.1038/cdd.2010.150.
[39] C. Chen, K.A. Ganar, S. Deshpande, On-chip octanol-assisted liposome assembly for bioengineering, J. Vis. Exp. 2023 (2023), https://doi.org/10.3791/65032.
[40] L. Van De Cauter, F. Fanalista, L. Van Buren, N. De Franceschi, E. Godino, S. Bouw, C. Danelon, C. Dekker, G.H. Koenderink, K.A. Ganzinger, Optimized cDICE for efficient reconstitution of biological systems in giant unilamellar vesicles, ACS Synth. Biol. 10 (2021), https://doi.org/10.1021/acssynbio.1c00068.
[41] M.C. Blosser, B.G. Horst, S.L. Keller, CDICE method produces giant lipid vesicles under physiological conditions of charged lipids and ionic solutions, Soft Matter 12 (2016), https://doi.org/10.1039/c6sm00868b.
[42] Y. Deng, Y. Wang, B. Holtz, J. Li, N. Traaseth, G. Veglia, B.J. Stottrup, R. Elde, D. Pei, A. Guo, X.Y. Zhu, Fluidic and air-stable supported lipid bilayer and cell-mimicking microarrays, J. Am. Chem. Soc. 130 (2008), https://doi.org/10.1021/ja800049f.
[43] X. Zhu, Z. Wang, A. Zhao, N. Huang, H. Chen, S. Zhou, X. Xie, Cell adhesion on supported lipid bilayers functionalized with RGD peptides monitored by using a quartz crystal microbalance with dissipation, Colloids Surf. B Biointerfaces 116 (2014), https://doi.org/10.1016/j.colsurfb.2014.01.032.
[44] S. Vafaei, S.R. Tabaei, N.J. Cho, Optimizing the performance of supported lipid bilayers as cell culture platforms based on extracellular matrix functionalization, ACS Omega 2 (2017), https://doi.org/10.1021/acsomega.7b00158.
[45] B. Ananthanarayanan, L. Little, D.V. Schaffer, K.E. Healy, M. Tirrell, Neural stem cell adhesion and proliferation on phospholipid bilayers functionalized with RGD peptides, Biomaterials 31 (2010), https://doi.org/10.1016/j.biomaterials.2010.07.104.
[46] A. Kilic, F.N. Kok, Peptide-functionalized supported lipid bilayers to construct cell membrane mimicking interfaces, Colloids Surf. B Biointerfaces 176 (2019), https://doi.org/10.1016/j.colsurfb.2018.12.052.
[47] M. Oliveira, O. Franco, J. Nascimento, C. de Melo, C. Andrade, Mechanistic aspects of peptide-membrane interactions determined by optical, dielectric and piezoelectric techniques: an overview, Curr. Protein Pept. Sci. 14 (2013), https://doi.org/10.2174/1389203713149990070.
[48] J.A. Jackman, N.J. Cho, Model membrane platforms for biomedicine: case study on antiviral drug development, Biointerphases 7 (2012), https://doi.org/10.1007/s13758-011-0018-2.
[49] S. Park, J.A. Jackman, N.J. Cho, Comparing the membrane-interaction profiles of two antiviral peptides: insights into structure-function relationship, Langmuir 35 (2019), https://doi.org/10.1021/acs.langmuir.9b01052.
[50] S. Piantavigna, G.A. McCubbin, S. Boehnke, B. Graham, L. Spiccia, L.L. Martin, A mechanistic investigation of cell-penetrating Tat peptides with supported lipid membranes, Biochim. Biophys. Acta Biomembr. 1808 (2011), https://doi.org/10.1016/j.bbamem.2011.03.002.
[51] A. Mechler, S. Praporski, K. Atmuri, M. Boland, F. Separovic, L.L. Martin, Specific and selective peptide-membrane interactions revealed using quartz crystal microbalance, Biophys. J. 93 (2007), https://doi.org/10.1529/biophysj.107.116525.
[52] K.E. Burns, T.P. McCleerey, D. Thévenin, PH-selective cytotoxicity of pHLIP-antimicrobial peptide conjugates, Sci. Rep. 6 (2016), https://doi.org/10.1038/srep28465.
[53] M. Rodahl, B. Kasemo, On the measurement of thin liquid overlayers with the quartz-crystal microbalance, Sens. Actuators A Phys. 54 (1996), https://doi.org/10.1016/S0924-4247(97)80002-7.
[54] A. Moshnikova, V. Moshnikova, O.A. Andreev, Y.K. Reshetnyak, Antiproliferative Effect of pHLIP-Amanitin, Biochemistry 52 (2013) 1171–1178, https://doi.org/10.1021/bi301647y.
[55] K. Mortezaee, B7-H3 immunoregulatory roles in cancer, Biomed. Pharmacother. 163 (2023), https://doi.org/10.1016/j.biopha.2023.114890.
[56] R.C. Adochite, A. Moshnikova, J. Golijanin, O.A. Andreev, N.V. Katenka, Y. K. Reshetnyak, Comparative study of tumor targeting and biodistribution of pH (Low) insertion peptides (pHLIP® Peptides) conjugated with different fluorescent dyes, Mol. Imaging Biol. 18 (2016), https://doi.org/10.1007/s11307-016-0949-6.
[57] X. Hu, J. Tan, S. Ye, Reversible activation of pH-responsive cell-penetrating peptides in model cell membrane relies on the nature of lipid, J. Phys. Chem. C 121 (2017) 15181–15187, https://doi.org/10.1021/acs.jpcc.7b03092.
[58] S. Munusamy, R. Conde, B. Bertrand, C. Munoz-Garay, Biophysical approaches for exploring lipopeptide-lipid interactions, Biochimie 170 (2020), https://doi.org/10.1016/j.biochi.2020.01.009.
[59] J.A. Jackman, R. Saravanan, Y. Zhang, S.R. Tabaei, N.J. Cho, Correlation between membrane partitioning and functional activity in a single lipid vesicle assay establishes design guidelines for antiviral peptides, Small 11 (2015), https://doi.org/10.1002/smll.201403638.